



Development of a Conductive Polypyrrole and Magnetic Ferrite Particles Decorated-Polyester Nonwoven Composite as an Electromagnetic Interference Shield Material

Burhan Beycan  0000-0002-2759-1985

Meryem Kalkan Erdoğan  0000-0002-2905-4438

Meral Karakışla  0000-0001-7036-094X

Mehmet Saçak  0000-0001-9395-8303

Department of Chemistry, Faculty of Science, Ankara University, Ankara, Tandoğan, Türkiye

Corresponding Author: Mehmet Saçak, sacak@science.ankara.edu.tr

ABSTRACT

Electromagnetic interference (EMI) shields have become more important because of the detrimental effects of electromagnetic radiation that are effective on systems, equipment, and even human health. High yields of conductive polypyrrole and magnetic (nano)particles (MPs) were consecutively placed on PET nonwoven to highlight this challenge. Surface resistance was measured to identify the influence of in-situ oxidative polymerization factors including oxidant content and MP deposition order. The MPs' magnetic properties and morphology were examined using Vibrating Sample Magnetometer (VSM) and Scanning Electron Microscopy (SEM). The electromagnetic shielding effectiveness (EMSE) and the relative shielding effectiveness (Re) and absorption (Ab) within the 30 MHz-3 GHz range were used to assess the textiles' EMI shielding properties. Accordingly, the most considerable absorption-dominant attenuation (74.7% at 2.20 GHz) and maximum EMSE value (6.60 dB) were found in the PET/PPy/Fe₃O₄ composite.

1. INTRODUCTION

The demand for life-facilitating electronic devices, such as microwave ovens, air conditioners, office tools in the workplace, and mobile phones, has steadily increased with developing technology. Communication tools and devices with many digital circuits cause energy emissions at different frequencies into the environment. Although these devices, which exist in all areas of our lives, make our daily work more accessible, they also cause electromagnetic pollution emitted by electromagnetic waves known as "electrosmog" to the environment. For example, due to the EM waves emitted by other devices, the electronic devices may not operate correctly, or some malfunctions may have occurred in commercial and military applications. It has also been reported that EM waves can also cause acute health risks to the human body, and depending on the frequency, electric and magnetic field intensities, direction, and polarization of these radiations, they can damage

human cells at different rates [1]. When EM waves fall on human tissue, some of the incoming waves penetrate more profoundly, while a large part of the remainder is absorbed, causing an increase in body temperature [2]. Consequently, shielding is required to protect human health against such hazards and prevent sensitive electrical devices from suffering harmful EM radiation.

With the proper shielding or absorption of EM fields, the EMI problem may be solved. To address this issue, conductive polymers such as PPy, polyaniline, and polythiophene, which are light and readily produced, are utilized. Those polymers with tunable conductivity both reflect and absorb radiation, and the shielding by absorption often being more significant than reflection [3]. Thus, conductive polymers coated on insulating substrates, such as textile-based materials, enable them to be used as a unique material for EMI shielding [4-16]. Kuhn et al. observed that the conductivity of the PPy-coated fabric was significantly influenced by the doping agents utilized and

To cite this article: Beycan B, Erdoğan M K, Karakışla M, Saçak M. 2024. Development of a Conductive Polypyrrole and Magnetic Ferrite Particles Decorated-Polyester Nonwoven Composite as an Electromagnetic Interference Shield Material. *Tekstil ve Konfeksiyon*, 34(2), 147-161.

the extent of doping during the fabrication process. Yildiz and colleagues conducted an experiment involving the vapor-phase polymerization of pyrrole on cotton yarn, utilizing different concentrations of ferric chloride as the initiator. The PPy-coated yarn was utilized in the production of a textile material. The experimental results indicate that fabric treated with an initiator concentration of 0.6 mol.L^{-1} exhibited a significant EMSE of 2 dB across the frequency spectrum ranging from 0 to 3 GHz. Using anhydrous FeCl_3 as the oxidant, Kalkan Erdogan et al. reported that the conductive PTh/PET composite fibers could be produced by in situ chemical polymerization and displayed an average 4 dB EMSE value between 1 and 3 GHz. Textile products such as PET, cotton, wool, viscose, cupro, and lyocell are frequently preferred in developing shield materials due to their outstanding properties, such as lightweight, cost-effective, facile processing, and availability.

EM waves can also be shielded using magnetic components such as ferrite nanoparticles with higher dielectric constant. These particles can also be combined with a conductive polymer to generate unique ferromagnetic conductive composites that impart electrical and magnetic capabilities to the composite [17-24]. Therefore, the composite's high conductivity and dielectric constant contribute to their excellent EMI shielding efficiency.

EMI shielding applications may benefit from conductive and magnetic textile composites manufactured using this innovative approach. To do this, in this work, we utilized PET nonwoven, a widely used industrial textile, practically transformed into an EMI shielding composite by depositing conductive PPy and different ferrites such as Fe_3O_4 , CoFe_2O_4 , and MnFe_2O_4 , on its surface, through facile successive process steps. Although other studies have also employed conductive PPy and different metal particles on textile substrates [25-30], our work is considerably distinct in several factors, such as selected preparation routes, usage of various MPs, and criteria for evaluating the performance. For example, in this study, we used a novel approach to assure a uniform and dense deposition of components onto the PET nonwoven, which could also be readily transferred to industrial applications. The PPy-coated polyester fabric may be viable for electronic component packaging. The conductivity property of PPy renders it a potential candidate for furnishing electrostatic discharge (ESD) safeguarding. Electrostatic discharge (ESD) is known to have detrimental effects on sensitive electronic components. However, using PPy-coated polyester fabric as an internal lining or wrapping material can effectively disperse static charges, thereby averting any potential damage that may arise during handling, transportation, or storage. Using PPy-coated polyester fabric in packaging may safeguard against electrostatic discharge, thereby protecting electronic components from voltage spikes that can result in malfunctions or permanent damage. Moreover, polyester textiles' flexibility and low mass facilitate its incorporation into diverse packaging configurations,

enabling effective and dependable packaging remedies for electronic commodities. We kept the usage of chemical reagents in the lowest sufficient amounts that could only be consumed to coat the surface. With the help of this, we intended to decrease the possible residues that would be formed in the solution, which require more water for elimination. In a very recent study published by our group, we also ensured the homogenous and dense decoration of conductive polyaniline and different ferrites onto the PP nonwoven by utilizing that technique [31]. We could obtain satisfactorily high conductive PP composite with the desired properties. Thus, in this study, we intended to transfer that experience to a new composite formed by a relatively thick PET texture. As a result, we sought to enhance the PET matrix's interaction with the conductive and magnetic components. Also, we tested the composites' EMI shielding performance in the 30 MHz to 3 GHz frequency band, which includes the wide radio and microwave frequencies generated by the potential everyday electronic gadgets.

2. MATERIAL AND METHOD

2.1 Material

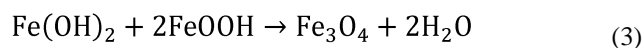
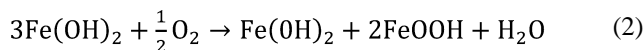
PET nonwoven fabric (weight 130 g/m^2) was purchased from KORDSA Company (Kocaeli, Turkey). The textiles were washed at 40°C for 1 hour in an aqueous solution comprising a reference detergent solution, whose details can also be found in our previous work [31]. After the washing procedure, the fabric samples were dried in a vacuum oven at 50°C and then conditioned in a desiccator. The chemicals, pyrrole (97%) (Fluka), APS (Fluka), NH_4OH solution (25%) (Atabay), NaOH (Sigma Aldrich), HCl solution (37%) (Merck), $\text{FeCl}_2 \cdot 4\text{H}_2\text{O}$ (Merck), $\text{FeCl}_3 \cdot 6\text{H}_2\text{O}$ (Merck), $\text{CoCl}_2 \cdot 4\text{H}_2\text{O}$ (Merck), and $\text{MnCl}_2 \cdot 4\text{H}_2\text{O}$ (Merck), were all received from the distributors of the companies in Turkey and used without performing further purifications.

2.2 Method

2.2.1 MPs synthesis by co-precipitation method

According to a published report in the literature, the MPs, including Fe_3O_4 , CoFe_2O_4 , and MnFe_2O_4 , were synthesized using the co-precipitation method [32]. Firstly, for Fe_3O_4 synthesis, 20 ml aqueous solutions of 0.30 M $\text{FeCl}_3 \cdot 6\text{H}_2\text{O}$ (1.18 g) and 0.15 M $\text{FeCl}_2 \cdot 4\text{H}_2\text{O}$ (0.46 g) were prepared by dissolving in two separate beakers. Then, these solutions were mixed in a round bottom two-necked flask with a gas inlet at 50°C under N_2 gas for 20 min. By dropwise adding 4.5 mL of NH_4OH solution to the mixture, the pH was adjusted to 11. The precipitation of the particles was monitored by the sudden color change from bright yellow to brownish black for 1h. After completing the reaction, the MPs were isolated from the solution using a magnet centrifuged four times at 8000 rpm with the distilled water

until a neutral solution (pH 7) was obtained. The formed of MPs is given in the supplementary file Figure 1s. The proposed formation mechanism of Fe₃O₄, which is formed due to the alkalization of iron ions, is provided in reactions (1-3).



The synthesis of the other MPs was also employed similarly to that of Fe₃O₄, except using 0.15 M MnCl₂·4H₂O and 0.15 M CoCl₂·4H₂O aqueous solutions prepared in 0.50 M 10 mL of HCl solutions, instead of 0.15 M FeCl₂·4H₂O. Briefly, after mixing Fe⁺³ and Me⁺² (either Mn⁺² or Co⁺²) solutions by keeping Fe⁺³/Me⁺² mol ratio 2/1, the aqueous solutions were stirred at 80°C under N₂ atmosphere for 20 min. Then, by the dropwise adding of 1.5 M aqueous NaOH solution until reaching pH 13, the precipitated CoFe₂O₄ and MnFe₂O₄ particles were isolated and washed similarly to that of Fe₃O₄ particles.

2.2.2 Preparation of PET/PPy nonwoven composite

The thickness of the PET nonwoven was measured as 0.895 mm before the treatments. PET nonwoven fabric with a dimension of 2x2 cm was introduced into a polymerization tube whose temperature was set to 20°C. The fabric samples were homogeneously impregnated with 0.15 M 1.2 mL of pyrrole solution prepared in 0.4 M HCl solution for 150 min. The in-situ oxidative polymerization was initiated by the dropwise adding of 1.0 mL various APS solutions (0.025 M-0.20 M) prepared in a 0.4 M aqueous HCl solution. After conducting in-situ polymerization for 2 hours, the PET/PPy composite removed from the medium was carefully washed with distilled water and ethyl alcohol to eliminate unreacted oxidant or monomer residues, respectively. Following redoping in 0.4 M HCl solution, the composite was dried for 24 h in a vacuum oven at 50 °C. The composite's PPy content (%) was evaluated

gravimetrically by comparing the fabric weights before and after polymerization.

2.2.3 Preparation of PPy and MPs deposited- PET nonwoven composites

The conductive and magnetic composite textiles were obtained in two distinct routes by altering the conductive PPy and MPs' sequence. The PET nonwoven fabric was impregnated with pyrrole monomer, followed by in-situ polymerization with APS oxidant and deposition of magnetic particles on the resulting PPy-PET composite. In the process of sequential addition, MPs were added in a specific order. PET fabric was initially saturated with MPs through dripping and impregnation. Following a 24-hour drying period, the PET/MP composite was impregnated with pyrrole monomer. Then, APS was utilized as an oxidizing agent in the in-situ polymerization process. Briefly, In the first route, PET nonwoven textiles was impregnated with magnetic particles using the drop coating procedure. Briefly, PET nonwoven textiles were uniformly impregnated with the 25 mg/mL aqueous MPs dispersions and dried in a vacuum oven at 50°C. Then, on a PET/MPs nonwoven composite, in-situ oxidative pyrrole polymerization was accomplished similarly to that of the PET/PPy composite. The composite sample was named PET/MPs/PPy. In the second route, PET fabric surface was impregnated with pyrrole monomer, followed by in situ polymerization with APS solutions of varying concentrations. On this group, MPs were deposited after a PET/PPy composite was generated, similar to a PET/MPs composite. The composite sample obtained by the second route was defined as PET/PPy/MPs. The schematic illustration for the preparation routes of each composite was provided in Figure.1. The thickness measurements of the composites prepared according to the order of addition of MPs were measured with Mitutoyo Digital Thickness Measurement Comparator and added to Table 1 and Table 2.

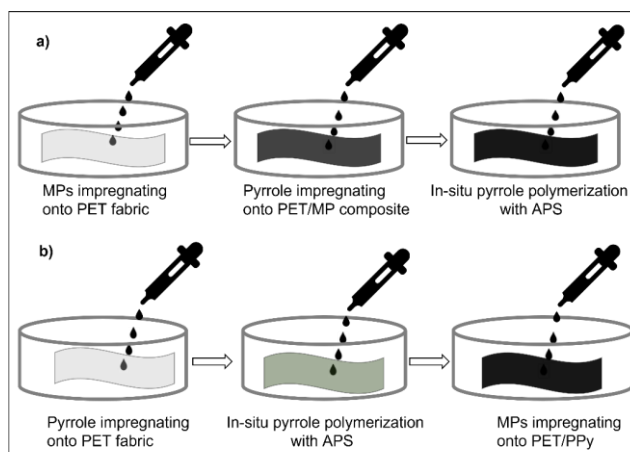


Figure 1. The preparation routes for a) PET/MP/PPy and b) PET/PPy/MP

2.3 Characterization

The fabric thickness of each sample was measured using a Mitutoyo digital thickness measurement comparator which can measure as mm. Optical light microscopy of samples were taken using Optika B-350 instrument. Water contact angles (CAs) were measured by a contact angle measurement device using 5 microliter water droplets. ATR-FTIR (Attenuated Total Reflection-Fourier Transform Infrared) Spectroscopy (BRUKER Alpha) was used to obtain PET fabric and PET/PPy composite materials' spectra. Depending on the magnitude of the surface electrical resistance, the surface resistivity measurements were performed by either a Thurlby 1503 digital multimeter or a Keithley 6517A high resistance meter, using the two-probe technique. The average of 10 different values obtained from the composite's various areas was used to calculate the composite's surface resistivity. The magnetic hysteresis and AC susceptibility of MPs were obtained using Cryogenic Limited's PPMS device with a NbTi magnet. After 3 nm of Au-Pd deposition, the composites' surface morphologies and semi-quantitative elemental content were taken using the Quanta 400F SEM equipment.

The EMSE measurements identified the EMI shielding performances of the conductive and magnetic nonwoven composites by following ASTM D 4935-18 standard. An Agilent E5061B Network Analyzer and an Electro-Metrics 2107A test fixture were utilized during the measurement. The EMSE of a composite was calculated according to Equation (1), whose details were given in the literature [33].

The electric fields of the transmitted and incident electromagnetic waves are denoted by E_t and E_i , respectively. The shielding failure of a sample was quantified using the Transmittance (T), and the shielding (attenuation) caused by electromagnetic wave reflections from the sample was identified by the Reflection (R_e). The composites' T and R_e magnitudes were determined using the Network Analyzer's S parameters. The absorption-induced attenuation (A_b) was also calculated using the composite's total R_e and T values in the following Equation (2-4):

$$\text{EMSE (in decibels dB)} = 20 \log \left(\frac{E_i}{E_t} \right) \quad (1)$$

$$R_e = \left| \frac{E_r}{E_i} \right|^2 = |S_{11}|^2 \text{ or } |S_{22}|^2 \quad (2)$$

$$T = \left| \frac{E_t}{E_i} \right|^2 = |S_{12}|^2 \text{ or } |S_{21}|^2 \quad (3)$$

$$I = A_b + R_e + T \quad (4)$$

3. RESULTS AND DISCUSSION

Figure 2 illustrates the connection between the surface electrical resistance and PPy content of the PET/PPy fabric composite generated by in-situ oxidative pyrrole polymerization of PET textiles with varying APS concentrations. Polymerizations were carried out in this manner by adding 0.2 M pyrrole solution dropwise and an APS-containing solution at concentrations ranging from 0.05 to 0.2 M. When the APS concentration was 0.15 M, the composite exhibited the lowest surface resistance value. Poor conductivity values were obtained at low APS concentrations due to the low PPy contents of the composite. When the APS concentration was increased to 0.15 M, the lowest surface resistivity value (the highest conductivity) was obtained as $0.15 \text{ k}\Omega \text{ cm}^{-2}$. With the further increment of APS concentration, the PPy content of the composite also increased, but the surface resistivity showed an increase as a possible result of over-oxidation [34, 35]. Carbonyl defects caused by high oxidation disrupt conjugation and obstruct charge transfer [36]. That is, carbonyl is another form of structural anomaly which can be found in PPy [37]. One possible explanation for reducing electrical conductivity is that carbonyl groups can arise through the process of over-oxidation of polypyrrole. Alternatively, they can be generated as a result of chain termination, which occurs when water molecule in APS solution attacks the pyrrole rings through nucleophilic attack [11, 26]. As such, carbonyl defects may be present at the β -carbon positions located in the middle of a chain or at the chain termini. It is evident that the disruption of conjugation occurs at pyrrole rings that possess carbonyl defects in both instances. As a consequence, electrical conductivity is reduced.

After establishing the conditions for forming homogeneous PPy coating on PET textiles, the effects of MPs deposition order were examined. Two distinct sets were created for efficient MPs and PPy deposition onto the PET nonwoven, comprising sequential MPs impregnation and PET deposition, and vice versa. As a result, the PET fabrics were impregnated with MP's dispersion in the first consecutive batch and then coated with conductive PPy (Table 1). After deposition of PPy onto the PET fabrics, the composites were impregnated with the appropriate proportions of MPs dispersions, as indicated in Table 2.

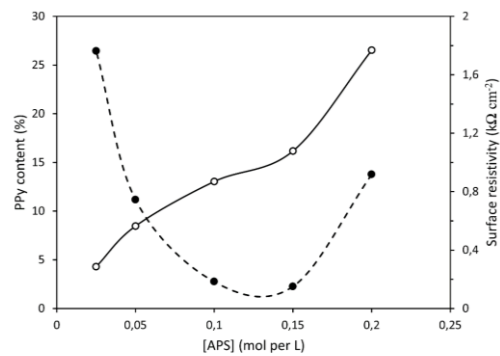


Figure 2. The changes in PPy content (%) and surface electrical resistivity of the PET/PPy composites with the APS concentration.

As shown in Table 1, the MPs contents (%) of PET/Fe₃O₄/PPy and PET/CoFe₂O₄/PPy composites were slightly lower than MnFe₂O₄ due to the comparatively delicate Fe₃O₄ and CoFe₂O₄ particle sizes in the dispersion and therefore removed from the composites. This fact is corroborated by the quick aggregation of MnFe₂O₄ particles on the PET surface, which results in a higher MPs content (%) for the composite. After the PPy deposition, although the PPy contents (%) of the composites did not significantly vary, the surface resistivity of the PET/MPs composites had different values. Surface resistivity values (0.543 kΩ cm⁻² – 0.939 kΩ cm⁻²) increased somewhat above those of a PET/PPy composite (0.15 kΩ cm⁻²), possibly due to the disruption of PPy chains caused by the MPs present on the composite. The MPs component does not seem to affect the conductivity value of the composites significantly. The literature found that it has a lower surface resistance (i.e., a greater conductivity value) than PPy/ Fe₃O₄ composites that are not coated onto the fabric [38]. It is reasonable to conclude that as the PPy component of the composite lowers due to the presence of ferrites, the conductivity decreases as well.

After the first PET/MPs/PPy composite series, the second consecutive PET/PPy/MPs series were also executed, whose results are presented in Table 2. Accordingly, using the subsequent MPs deposition method, the composites' MPs contents (%) followed the same pattern as the first set; meanwhile, the MnFe₂O₄ particles provided the highest MPs content (%) to the composite. It was found that when the PPy content of the composite slightly decreased, the amounts of MPs that entered the composite raised, and as a result, the surface resistivity of the composite increased as well. After the Fe₃O₄ deposition, the highest conductivity of

the composite was obtained as 0.8237 kΩ cm⁻². In general, the composite conductivity fell as the ratio of conductive polymer to MPs dropped, or the amounts of MPs in the composite grew, as compatible with the literature [19]. Because of MPs' relatively lower conductivity values, MPs had a reverse effect on the conductivity of the composites. Thus, this may have partially hindered the creation of conduction paths.

Upon observation of the optical microscope images in Figure 3, it is observed that the fibers exhibit accumulations following impregnation of the ferrites with PET fibers. Furthermore, ferrites adhere to the fibers, resulting in a brown-black color on the fiber's surface. In contrast, the results of in-situ pyrrole polymerization on PET fiber reveal a uniform dispersion of the polymer on the fibers. At higher magnifications, the interaction between the fibers is observed rather than on the fibers themselves, as seen in the case of ferrites. The presence of fiber is observed to be surrounded within them.

In Figure 4, the spectra were acquired utilizing an ATR-FTIR Spectroscopy to employ PET fabric and PET/PPy composite materials. Figure 4 displays the ATR-FTIR spectra of both PET fabric in its pure form and the PET/PPy fabric composite. The spectral bands observed at the 1715 cm⁻¹ band indicate the C=O group of PET fabric [39, 40]. The band detected at 1242cm⁻¹ can be attributed to the -COO- stretch of the ester group. However, in PET/PPy composite, that band almost disappeared. The existence of PPy can be verified by the peak at 1556 cm⁻¹ that follows, which is associated with the stretching vibration of the C=C ring in pyrrole [41]. Also, C-H bending vibration bands exhibited by PPy are observed at wavenumbers of 1017 cm⁻¹.

Table 1. The surface resistivity, MPs contents (%), and PPy contents (%) of the PET/MPs/PPy composites formed by sequential deposition of MPs and PPy.

| MPs TYPE | THICKNESS (PET/MPs) (mm) | SURFACE RESISTIVITY (PET/MPs) (MΩ CM ⁻²) | MPs CONTENT (%) | PPy CONTENT in PET/MPs (%) | THICKNESS (PET/MPs/PPy) (mm) | SURFACE RESISTIVITY (PET/MPs/PPy) (KΩ CM ⁻²) |
|----------------------------------|--------------------------|--|-----------------|----------------------------|------------------------------|--|
| Fe ₃ O ₄ | 1.083 | 67.59 | 15.62 | 9.82 | 1.182 | 0.939 |
| CoFe ₂ O ₄ | 1.040 | 989.20 | 17.90 | 8.76 | 1.166 | 0.543 |
| MnFe ₂ O ₄ | 0.997 | 159.980 | 20.56 | 19.13 | 1.113 | 0.650 |

*The thickness of PET nonwoven fabric was ~0.895 mm

Table 2. The surface resistivity, PPy contents (%), and MPs contents (%) of the PET/PPy/MPs composites formed by sequential deposition of PPy and MPs.

| MPs TYPE | PPy CONTENT in PET (%) | SURFACE RESISTIVITY (PET/PPy) (KΩ CM ⁻²) | MPs CONTENT (%) | THICKNESS (PET/PPy/MPs) (mm) | SURFACE RESISTIVITY (PET/ PPy/MPs) (KΩ CM ⁻²) |
|----------------------------------|------------------------|--|-----------------|------------------------------|---|
| Fe ₃ O ₄ | 16.17 | 0.142 | 14.97 | 1.049 | 0.8237 |
| CoFe ₂ O ₄ | 16.12 | 0.151 | 13.43 | 1.167 | 0.9178 |
| MnFe ₂ O ₄ | 12.95 | 0.131 | 16.71 | 1.180 | 1.9193 |

*The thickness of PET nonwoven fabric was ~0.895 mm and PET/PPy was ~1.031 mm



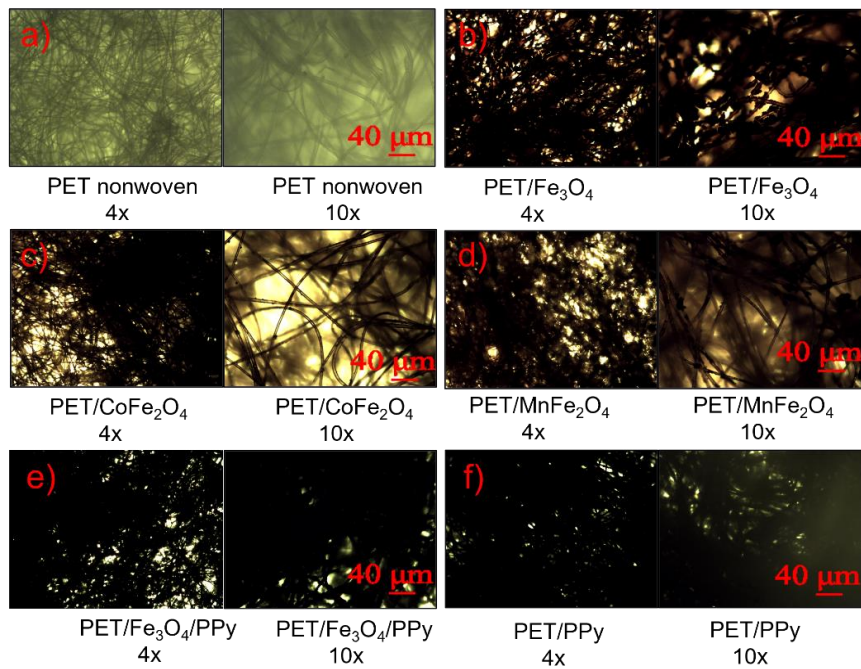


Figure 3. Optical light microscopy images of pure PET nonwoven and its composites with MNPs and PPy
*The polymerization conditions at [PPy] = 0.1 M and [APS] = 0.15 M

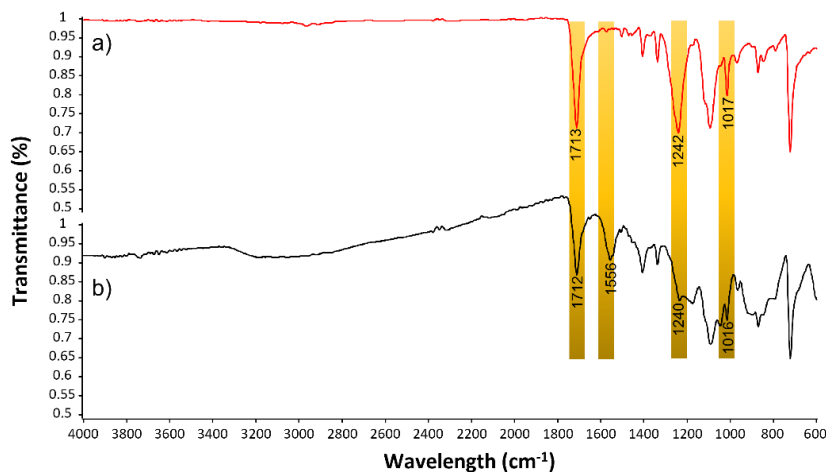


Figure 4. FTIR spectrum of a) PET nonwoven fabric and b) PET/PPy composite.
*The polymerization conditions at [PPy] = 0.1 M and [APS] = 0.15 M

3.1 Surface Wettability

The determination of contact angle values for different composites of PET nonwoven fabric is a useful approach to gain knowledge about their surface properties and wettability features. The comparative analysis of contact angle measurements can facilitate the clarification of the influence of distinct variables, such as magnetic particles and in-situ pyrrole polymerization, on the hydrophobic properties of composite surfaces. Consequently, attempts have been made to determine the hydrophilicity of the PET nonwoven after the successive coating procedures using the water contact angle measurements. In Figure 5., PET nonwoven fabric displays a contact angle (CA) value of 160°, which is the highest among the samples. This indicates that the fabric possesses hydrophobic

characteristics and has a low surface energy. The observed high contact angle value implies that water droplets exhibit a tendency to assume nearly spherical shapes on the surface of pure PET fabric.

Ferrite nanoparticles typically exhibit slight hydrophobicity [43]. The incorporation of Fe₃O₄ nanoparticles into PET fabric results in a reduction of the contact angle to 136°, which suggests an enhanced hydrophilic nature in comparison to the unmodified PET fabric. The reduction in contact angle indicates enhanced wettability attributed to the existence of Fe₃O₄ which has the potential to alter the surface energy of the fabric. The impregnation of ferrite particles which is in the form of aqueous solutions onto PET fabric surface results in a reduction of hydrophobicity, which is attributed to the hydrophilic contribution provided

by the ferrite nanoparticles. The same reduction pattern was seen on the incorporation of CoFe_2O_4 and MnFe_2O_4 to the PET fabric whose contact angle values are 119° and 109° , respectively. The hydration of ferrite particles in aqueous systems leads to the formation of Fe-OH groups on their surfaces, which consequently causes a reduction in their hydrophobic nature [44]. Also, the order of MP sizes within the composites can offer a more comprehensive and coherent evaluation of the contact angle measurements. The present study indicates the sequence of nanoparticle sizes as $\text{MnFe}_2\text{O}_4 > \text{CoFe}_2\text{O}_4 > \text{Fe}_3\text{O}_4$. The trend of the contact angle values in the composites, in comparison to pure PET, is observed to follow the order of nanoparticle sizes. MnFe_2O_4 nanoparticles, which are the largest in size, exhibit a significant influence on the contact angle, leading to a reduction in its magnitude as compared to that of pure PET. The observed reduction may be ascribed to the amplified surface area and altered surface energy resulting to the existence of larger MnFe_2O_4 nanoparticles, thereby enhancing its wettability. The addition of Fe_3O_4 onto PET fabric surface results in the formation of nearly spherical water droplets due to the smallest particle size of the synthesized ferrites. This observation indicates that the incorporation of Fe_3O_4 particles has a negligible impact on the contact angle of the composite.

The in-situ polymerization of pyrrole results in a decrease in the contact angle value of the PET/PPy composite which is 149° . The possible explanation of this phenomenon could be attributed to the higher doping level of the PPy chains by the contribution of higher amounts Cl^- counter dopant anions during in-situ polymerization of pyrrole. Upon comparing the impact of Fe_3O_4 and PPy on the contact angle of PET fabric surface, it can be said that the slightly hydrophobic properties and aqueous solution of ferrites led to a greater reduction in their contact angle values. Consequently, the PET/MP exhibited a greater reduction in hydrophobicity. The study revealed that the sequencing of the incorporation of polypyrrole into the PET fabric as a composite and addition of MPs onto the PET fabric surface exhibited similar effects with regards to the contact angles of the composites. Figure 6 displays optical images captured from three discrete positions of a water droplet situated on a composite surface composed of PET/PPy/ Fe_3O_4 . In each of the three instances, a circular formation of water droplets with a high degree of symmetry is seen on the surface. The observed contact angle of 140 degrees is indicative of a near superhydrophobic state. However, upon reversing the fabric surface, it becomes apparent that the water droplet does not exhibit a slipping behavior.

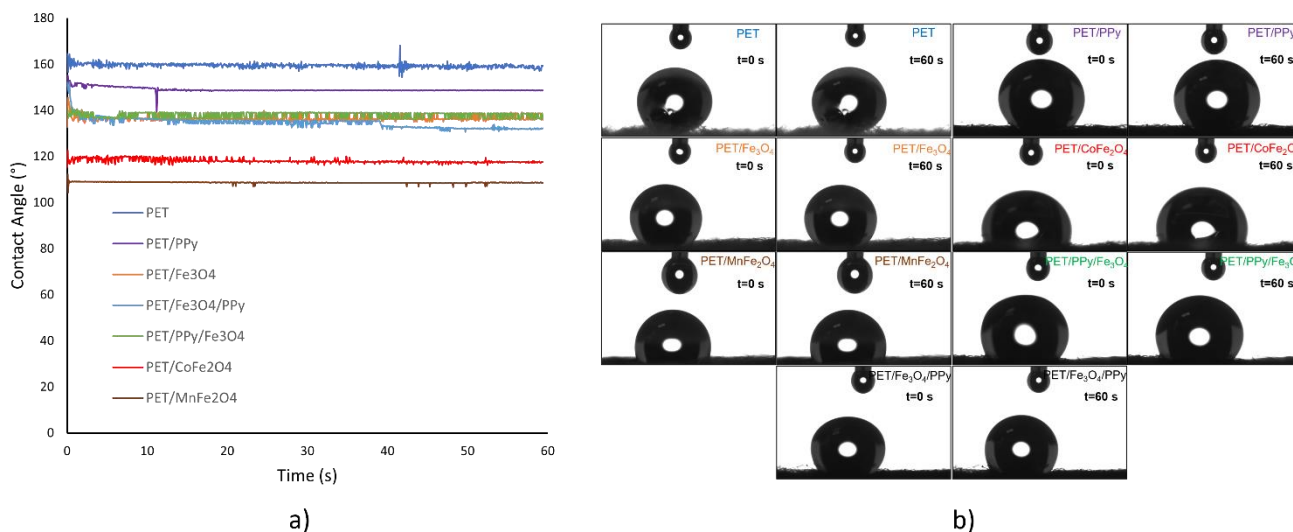


Figure 5. (a) CAs values pure PET nonwoven and its composites with MNPs and PPy. (b) their static water droplet's images at the beginning and final states.
*The polymerization conditions at $[\text{PPy}] = 0.1 \text{ M}$ and $[\text{APS}] = 0.15 \text{ M}$



Figure 6. Optical images from three distinct positions of a water droplet on a PET/PPy/ Fe_3O_4 composite surface.
*The polymerization conditions at $[\text{PPy}] = 0.1 \text{ M}$ and $[\text{APS}] = 0.15 \text{ M}$

3.2 VSM results

To reveal the imparted magnetic characteristic of the MPs that were synthesized by the co-precipitation method to the textile composite, the VSM measurement was performed at room temperature. The magnetic saturation values (M_s) of Fe_3O_4 , $CoFe_2O_4$, and $MnFe_2O_4$ particles employed in that study were previously found as 63.9, 16.5, and 44.2 emu per g, respectively [31]. These values were consistent with the values in the literature correlating the M_s values with the MPs' particle sizes because it has been reported that M_s values of the MPs are highly influenced by particle size and decrease with decreasing particle size [46, 47]. The behaviors of the MPs in the presence of a magnet are shown in the supplementary file Figure 2s. Ferrites are a material that exhibits magnetic properties due to its inherent magnetization. The magnitude of magnetization indicates the capacity of a substance to acquire magnetism when subjected to an extrinsic magnetic field. A greater magnetization value indicates an increased magnetic responsiveness and a higher potential for interacting with and reducing magnetic fields.

The comparative magnetic hysteresis results of Fe_3O_4 particles with the PET/ Fe_3O_4 and PET/ Fe_3O_4 /PPy composites are illustrated in Figure 7. As seen from the figure, due to the possible lower contribution of Fe_3O_4 to the composite, the M_s values of PET/ Fe_3O_4 (6.92 emu per g) and PET/ Fe_3O_4 /PPy (0.076 emu per g) took relatively low values compared to Fe_3O_4 particles (63.9 emu per g). This result is more than twice as high as the value found in comparative research published earlier in the literature [48]. The reduced magnetism value of the PET/ Fe_3O_4 composite is due to a proportionate reduction in the MPs amount contributing to magnetism because of non-magnetic materials such as PET fabric in the composite. Therefore, resulting in a proportional decrease to a lower magnetism value.

In contrast to Fe_3O_4 's M_s value of 63.9 emu per g, there was a substantial change in the saturation magnetization of the PET/ Fe_3O_4 /PPy composite that exhibited a narrow-sized-low magnetism with a M_s of 0.076 emu per g; thus, indicating a weak ferromagnetic activity. The magnetic properties of PPy/ Fe_3O_4 as determined in the literature without the use of PET fabric are comparable to those of the PET/PPy/ Fe_3O_4 composite used in our investigation [17]. This dramatic decrease in saturation magnetization might result from MPs being encapsulated in PPy. The polymer coating on these samples could explain these properties, such as low coercivity and saturation magnetization, which might be used in EMI shielding applications. It acts as a barrier to the exchange contact between the magnetic sublattices of the magnetic core (Fe_3O_4) in the oxide-polymer composite. In a composite framework, conductive polymer limited the MP's random mobility and interactions. This observation might be explained that magnetic Fe_3O_4 contributes more diminutive than the other components, PET and PPy.

MPs have superparamagnetic characteristics when analyzed with VSM. This property is owing to the particles' tiny size, the magnetic field's high saturation magnet, and the lack of coercive forces. Additionally, PET/ Fe_3O_4 and PET/ Fe_3O_4 /PPy composites have lower saturation magnetization values than pure Fe_3O_4 because of the contribution of non-magnetic elements in the composites.

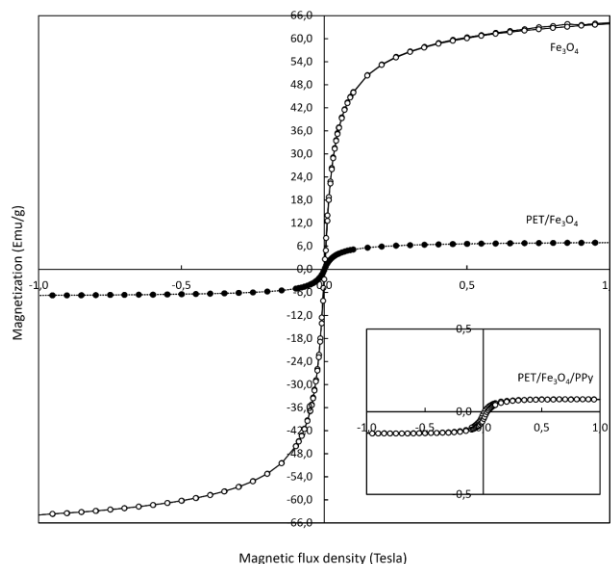


Figure 7. Magnetization values of Fe_3O_4 particles and PET/ Fe_3O_4 composite. Inset shows the magnetization of a PET/ Fe_3O_4 /PPy composite. *The polymerization conditions at [PPy] = 0.1 M and [APS] = 0.15 M

3.3 SEM-EDX

Figures 8–11 depict the morphological evaluation of the samples in the sequence of their emergence. As seen in Figure 8, when contrasted to the PET fabrics' sleek surface, it can be clearly evidenced that the surface of the composite fibers was heavily coated with the PPy polymers. It is apparent from the micrographs taken at the higher magnifications (Figure 8d and 8e) that the PPy coat took a dense and thick state and made a layer-like texture by overlapping the PPy polymers to form piles on the fiber surfaces. It is worth mentioning that PPy polymers coated on the composite fibers developed heaps in the shape of spherical particles both individually and in groups. This morphology of the PPy coating on the PET surface is consistent with the earlier reports that employed APS as an oxidant (Figure 8e) in the literature [9]. Agglomerated structures can be observed on certain regions of the fiber surface. A plausible explanation for the formation of agglomerates could be attributed to the elevated concentration of pyrrole monomers in specific locales within the reaction mixture [44]. Oligomers can react with one another to contribute to forming agglomerations during the polymerization process. Oligomers are short chains of polymerized monomers that have undergone some degree of polymerization but are not fully grown polymer chains. When oligomers are present in the reaction mixture, they can act as reactive species that can continue to polymerize

by reacting with other oligomers or monomers. This process is known as chain-growth polymerization. If the reaction conditions are favorable, such as an adequate pyrrole concentration and a suitable temperature, the oligomers can undergo further polymerization by reacting with other nearby oligomers or monomers. As the oligomers react with one another, they can form larger polymer chains, leading to the growth of agglomerations within the reaction mixture. The agglomerations may arise from the association of multiple oligomers or partially polymerized chains, forming larger clusters or aggregates.

To comparatively evaluate the texture of MPs deposition after or before the PPy coating onto the PET surface, the SEM micrographs and EDX spectra of PET/MPs composites were also taken. The results are represented in Figure 9. First, it could be said that the composite comprising $MnFe_2O_4$ particles showed symptoms of aggregation, while Fe_3O_4 and $CoFe_2O_4$ particles were spread across the surface in a more dispersed manner. $MnFe_2O_4$ particles are also apparent on the surface, but the other MPs are more sparsely distributed. As provided in Figures 9a-9c, it can be understood that the individual Fe_3O_4 particles have the smallest particle sizes of all the particles, leading to a stained appearance to the PET fibers [50]. The rounded shape of the $MnFe_2O_4$ particles in the PET/ $MnFe_2O_4$ composite (Figure 9i-9k) micrographs is also thought to be striking. As compatible with the previous XRD crystallite size findings, the largest particle size was of the MPs on the PET fibers were found for $MnFe_2O_4$ with a diameter of 30.9 nm, followed by $CoFe_2O_4$ (16.4 nm) and Fe_3O_4 (11.5 nm), respectively. Additionally, Fe, Co, and Mn atoms were in the predicted atomic ratios (Fe/Me=2/1) in the EDX spectra. Due to the relatively large mesh size of the PET nonwoven fabric, the MPs are found to be deeply

embedded within its structure. While PPy exhibits an affinity for adhering to the fiber's surface, MPs generally tend to aggregate within the pores. Initially, the pores of the PET nonwoven fabric surface are filled with PPy through in-situ oxidative pyrrole polymerization. Subsequently, adding MPs to the PPy achieves the optimal EMSE value.

When the micrographs of PET/MPs/PPy are evaluated (Figure 10), it could be mentioned that the composite fibers are heavily decorated by the thick layers of MPs/PPy. The unique structure of PPy can also readily be observed in the micrographs in Figures 10c, 10g, and 10k (at higher magnifications), even in the presence of MPs deposition. Also, it was possible to separate the coating texture of MPs and PPy morphologically due to the relatively compact structure of PPy. Consequently, it can be deduced that the PPy polymers adhered to the PET fabric, and MPs were placed on top of or between these PPy coating. In other words, MPs may be incorporated in the PPy layer, or PPy was coated on the surface of the MPs. The electrical conductivity of PET/MP/PPy composites is hindered by the insulating behavior of ferrite particles located on their surface, which impedes charge transfer and blocks surface conductivity [23]. In the EDX spectra of the PET/MPs/PPy samples, the respective Fe, Co, and Mn atoms were all determined, which approves the existence/contribution of MPs in the composites. While the structure of Fe_3O_4 and $CoFe_2O_4$ particles contributed to the composites was almost identical, the $MnFe_2O_4$ particles seemed to have rod-like forms at low magnification. However, it resembles a human tooth at higher magnification [50]. Incorporating ferrite particles can disrupt the continuity and regularity of the conjugated chain, leading to the obstruction of the conducting path. In addition, the collaboration between the ferrite particles and the PPy chain may reduce the polymer chain's electronic density, ultimately resulting in a decline in conductivity [51].

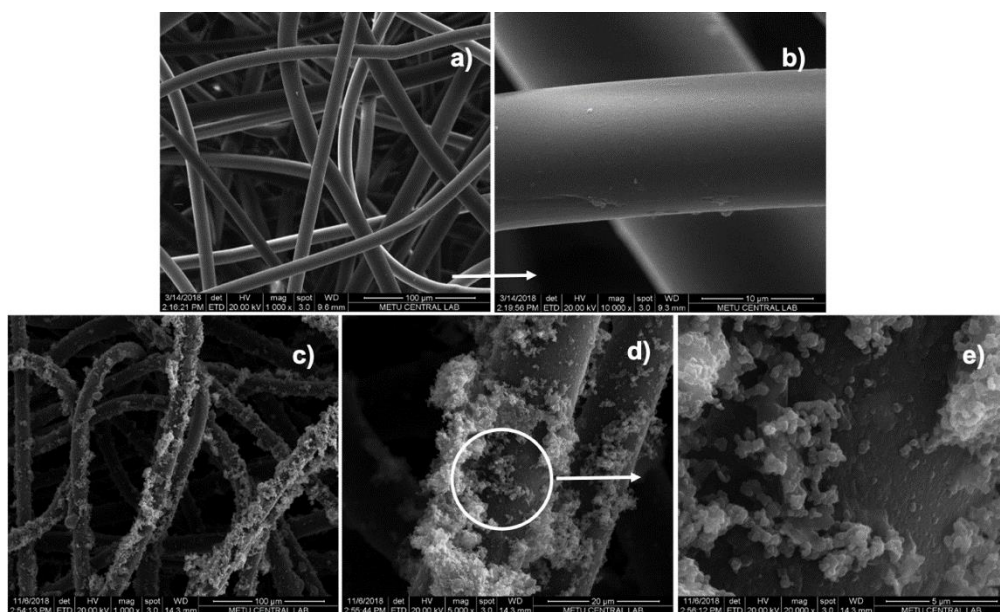


Figure 8. SEM micrographs of a) and b) fibers of PET nonwoven, c)-e) PET/PPy composite taken at different magnifications.

*The polymerization conditions at $[PPy] = 0.1$ M and $[APS] = 0.15$ M

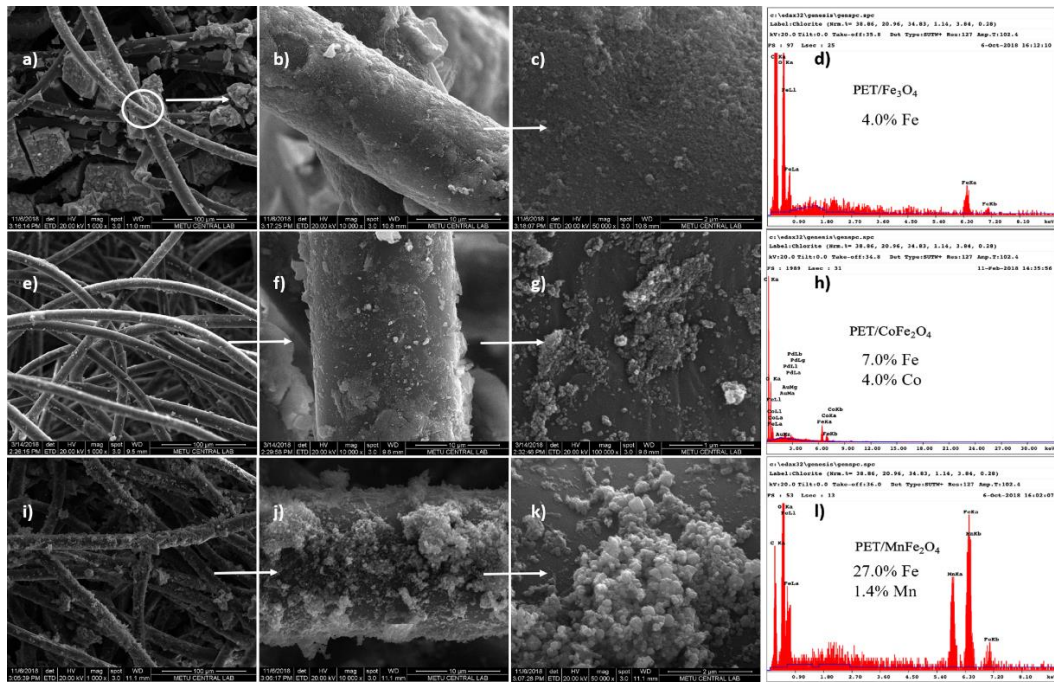


Figure 9. SEM-EDX results of PET/MPs composites: a)-d) PET/Fe₃O₄, e)-h) PET/CoFe₂O₄, and i)-l) PET/MnFe₂O₄.

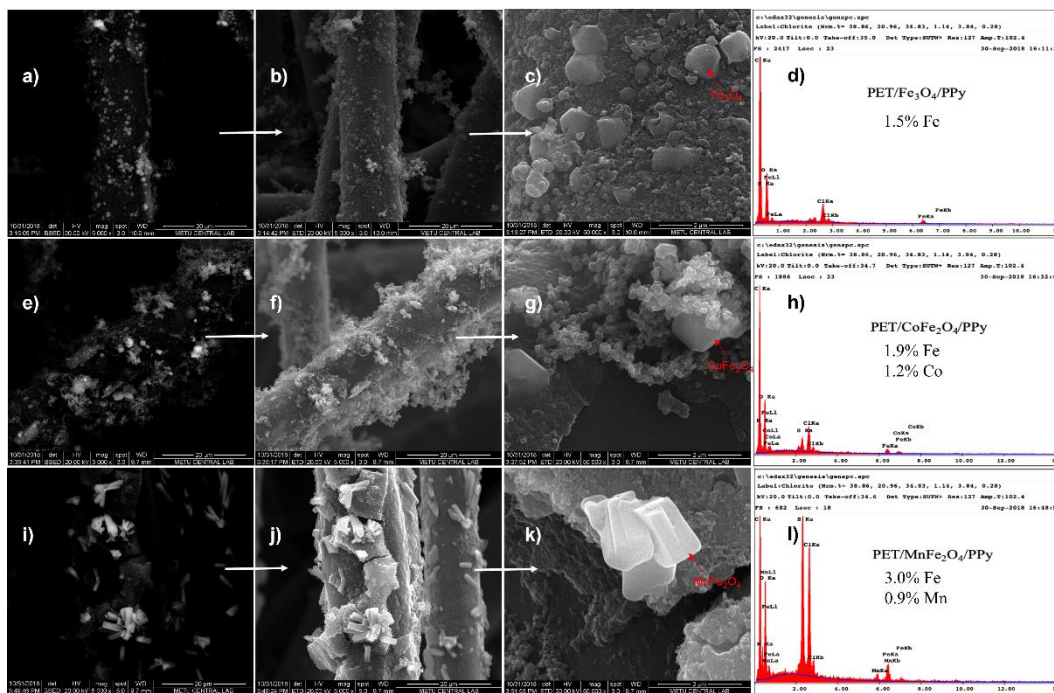


Figure 10. SEM-EDX results of PET/MPs/PPy composites a)-d) PET/Fe₃O₄/PPy, e)-h) PET/CoFe₂O₄/PPy, and i)-l) PET/MnFe₂O₄/PPy.
*The polymerization conditions at [PPy] = 0.1 M and [APS] = 0.15 M

Figure 11 shows sequential SEM micrographs of MPs-impregnated PET/PPy composites. The brightness exhibited by metallic particles serves as evidence for the existence of ferrites on the surface of PET fabric. The micrographs show that MPs were concentrated in some PET/PPy surface regions without forming an interaction. The composites exhibit a random distribution of ferrite particles, while the PET fibers are uniformly coated with PPy. The ferrites were observed to be either coated on the PPy, resulting in

the formation of composites with ferrite in the core, as exemplified by PET/CoFe₂O₄, or formed on the PPy, as demonstrated by PET/MnFe₂O₄, based on their corresponding particle sizes. Also, impregnation of MPs onto the PET fabric surface results in the observation in Figure 11, which subsequently leads to a reduction in the electrical conductivity of the composites in Table 2. According to the results of this study, MPs' coating morphology may also be readily distinguished from the

texture of PET in the PET/PPy/MPs composites. Fe_3O_4 and MnFe_2O_4 particles could be recognized in the micrographs at higher magnification (Figures 11c, 11k); however, the morphological distinction of CoFe_2O_4 and PPy could not be differentiated with a significant precision (Figure 11g). The Fe, Co, and Mn atoms could also be detected in the EDX spectra PET/PPy/MPs composites.

3.4 EMSE results

To evaluate the EMI shielding ability of the developed composites, the EMSE measurements were carried out between 30 MHz to 3 GHz frequency range, and the findings are successively presented in Figures 12 and 13. Figure 12 illustrates the significant impact of PPy on PET fabric, which exhibits the highest degree of conductivity, on the EMSE values. As seen in Figure 12, the PET/PPy composite had an average 3.2 dB EMSE value (the highest value 3.9 dB at 2.20 GHz), which translates to an average of 71.46 % EMI attenuation through the primary absorption mechanism (Ab: 67.9 %, Re: 3.56 %,).When the EMSE values of composites made with conductive polymers are studied, it is discovered that they protect mainly through the absorption mechanism. Due to the spherical nature of the PPy deposited onto the PET surface (in Figure 8), the incoming waves' energy is reduced. The aggregation of spherical particles results in cauliflower-like formations, which contribute to the attenuation of electromagnetic radiation [52]. This obtained EMSE value of the PET/PPy composite provides relatively higher protection against EMI than a similar study employing PPy deposited-textile composite in the literature[8].

It is noteworthy that PPy exhibits a remarkable absorption capacity, which enables it to transform electromagnetic energy into thermal energy via resistive heating. The electrical conductivity of the composite is a crucial factor in determining the effectiveness of EM shielding. In other words, a material's electrical conductivity directly impacts its capacity to transmit and disperse electric currents generated by EM fields, which in turn influences its ability to provide shielding. In EM shielding, greater conductivity values are typically favored due to their ability to redirect and disperse EM energy effectively. The potential of conducting PPy to serve as a conductive pathway for the dissipation of EM energy is the reason for its electromagnetic shielding effectiveness. The delocalization of electrons along the polymer chains in PPy is facilitated by its conjugated polymer structure, leading to a notable increase in electrical conductivity (Figure 2). The electrical conductivity exhibited by PPy enables it to function as an effective barrier against electromagnetic interference by absorbing and dissipating the incoming electromagnetic waves. That is, incorporating composites into PPy results in creating a highly conductive path that can efficiently divert and absorb electromagnetic energy, thereby reducing its impact on the shielded environment. The alignment and distribution of magnetized particles can be influenced by the composition and structure of the ferrite composite, thereby affecting its capacity to isolate and redirect magnetic fields. The interaction between magnetic particles and incident magnetic fields can be influenced by particle size and arrangement, which can impact the shielding performance.

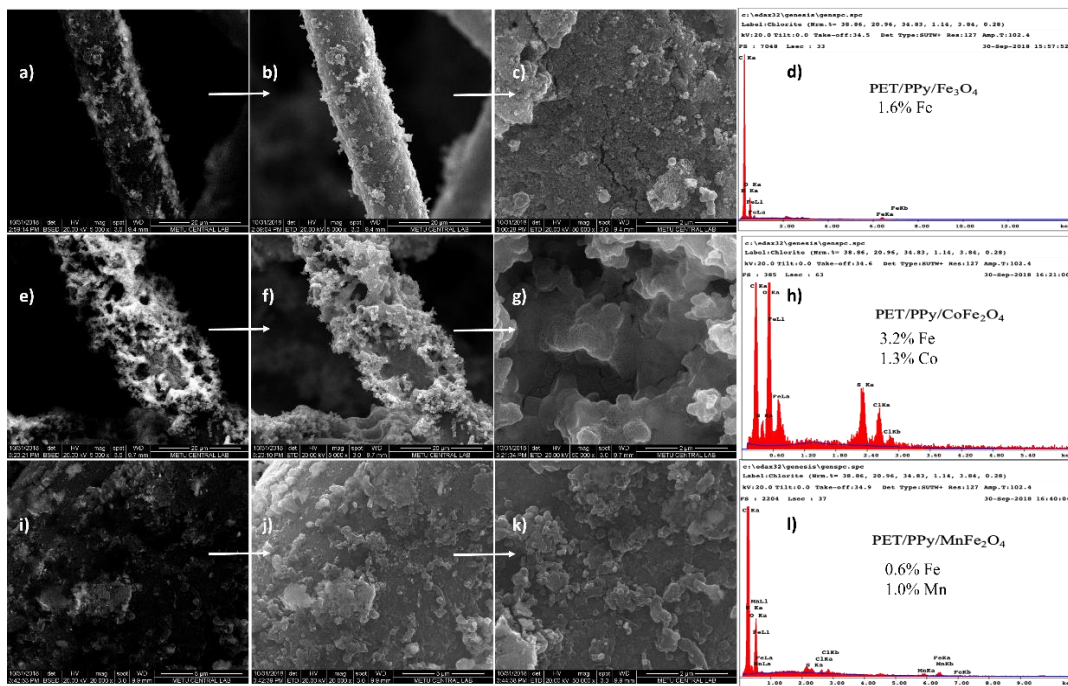


Figure 11. SEM-EDX results of PET/PPy/MP composites a)-d) PET/PPy/ Fe_3O_4 , e)-h) PET/PPy/ CoFe_2O_4 , i)-l) PET/PPy/ MnFe_2O_4 .
*The polymerization conditions at $[\text{PPy}] = 0.1 \text{ M}$ and $[\text{APS}] = 0.15 \text{ M}$

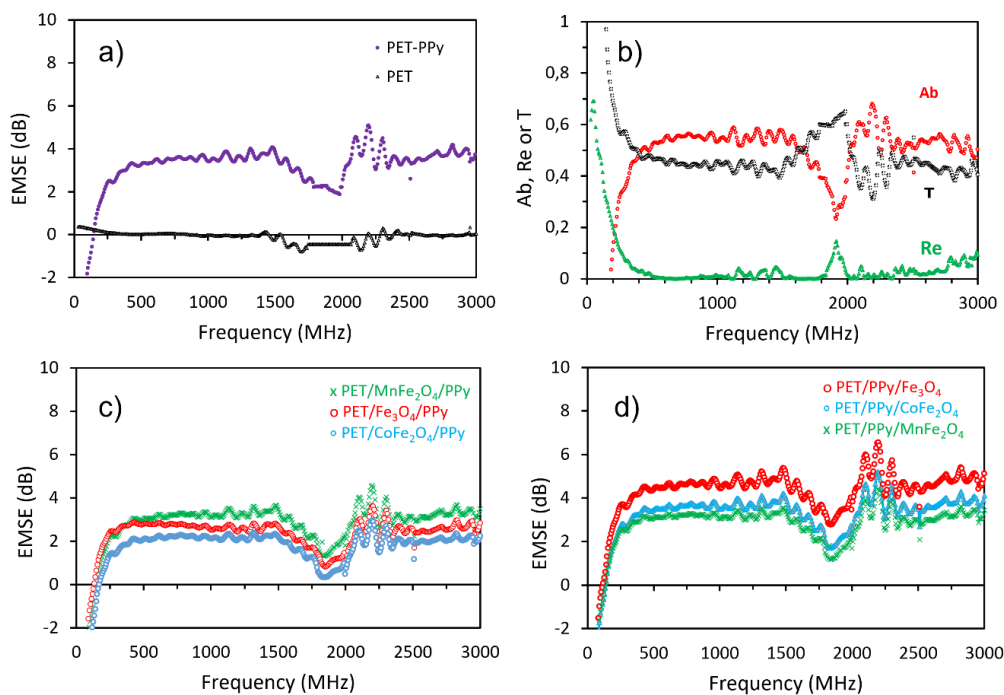


Figure 12. EMSE results of the composites, a) PET nonwoven and PET/PPy composite, b) Ab, Re, or T relative shielding efficiency of PET/PPy, c) PET/MP/PPy composites, and d) PET/PPy/MP composites.

When the results of MPs incorporated-PET/PPy composites are comparatively discussed with that of PET/PPy (Figure 12c and 12d), it was observed that the EMSE values varied depending on the deposition order of the MPs. For example, the PET/PPy has a lower protection value than the composites made after the addition of MPs but a better protection value than composites created before MPs deposition. If each series is compared, the EMSE values of the PET/PPy/MPs composites took relatively high values than the PET/MPs/PPy series, indicating a better EMI shielding performance in the selected frequency range. The composite containing Fe_3O_4 was found to have the greatest EMSE (6.60 dB at 2.20 GHz) in the PET/PPy/MPs series. In contrast, composite containing MnFe_2O_4 was found to have the highest EMSE (4.6 dB at 2.20 GHz) for the series of initial MPs deposition (PET/MPs/PPy).

Based on these calculations, the relative shielding efficiency (Ab and Re) and attenuation loss (T) values of the MPs-containing composites were also determined, and the sequential results are presented in Figure 13. Accordingly, the PET/PPy/MPs composite series with relatively greater EMSE values provided slightly more EMI attenuation than other PET/MPs/PPy composites (Figure 13). At 2.20 GHz, the PET/PPy/ Fe_3O_4 composite exhibits the maximum absorption of 74.7% and reflection of 5.7%. While the PET/PPy/MPs composite series has the highest total attenuation value of 80.4%, the other series has a value of approximately 50%.

PET/PPy/ Fe_3O_4 composite gives superior protection to the magnetic particle and polymer-coated cloth that has been described in the literature [28]. Adding Fe_3O_4 and CoFe_2O_4

nanoparticles to PET/PPy composites results in better levels of EM protection than using the materials in their pure state. It can be said that when materials containing MPs come into contact with electromagnetic waves, they alter the direction of these waves, diminishing them and therefore protecting the composite. Also, the addition of MPs to composites causes an increase in the dielectric constant value. It has been reported that this contributes to the rise in the absorption value by increasing the impedance matching level [53, 54]. Another factor that increases microwave absorption is the conversion of some of the incoming energy into heat [55].

Although the ground fabric material differed from the literature, we can practically make the comparison since the magnetic components (CoFe_2O_4) are the same. When the results are compared with a recent study published by Yörük et al., it can be seen that similar results ($\approx 900 \text{ M}\Omega$) were achieved in the present investigation, 918.20 $\text{M}\Omega$ (in Table 2), which shows that cobalt ferrite has insulating properties. Upon examination of SEM-EDX images (Figure 9-11), it is observed that the introduction of cobalt ferrite to the composite material, followed by the in-situ polymerization of pyrrole, leads to a reduction in the concentration of CoFe_2O_4 within the composite (PET/ CoFe_2O_4 /PPy), as compared to its subsequent addition to the composite (PET/PPy/ CoFe_2O_4). The reduction of conductivity line blockage in the composite material led to an increase in its overall conductivity.

However, the fabric utilized in the study above exhibited narrow pore sizes. Due to the relatively large pore sizes employed in the present study, the ferrite particles

aggregated within the gaps between them rather than remaining on the surface. Following the deposition of the conductive polymer, the ferrite particles are introduced into the solution, facilitating the transmission of electromagnetic (EM) waves and subsequently leading to a reduced EMSE value (2.92 dB). However, in the opposite coating route, the deposition PPy followed by ferrite deposition between the gaps of PET nonwoven enabled the interaction of polymer fibers that yields relatively higher EMI shielding (5.1 dB).

Also, Yörük et al. found that after the deposition of CoFe_2O_4 on the polypropylene nonwoven, it was observed that surface resistivity was measured almost at $900 \text{ M}\Omega$ compared to the Fe_3O_4 which was nearly as $55 \text{ M}\Omega$ that reveals that the conductivity of CoFe_2O_4 is remarkably low to that of Fe_3O_4 particles. Hence, it was observed that the composite material incorporating Fe_3O_4 exhibited superior efficacy in shielding against EM waves and demonstrated a higher EMSE value.

The PET/PPy/ MnFe_2O_4 composite and the PET/ MnFe_2O_4 /PPy composite exhibit comparable protection levels, indicating that the sequence in which MnFe_2O_4 particles are added has no significant effect on the EMSE values. This observation may have arisen from the limited ability of MnFe_2O_4 particles to adhere to the fabric surface during composite fabrication. Inadequate PPy deposition on the PET fabric surface can be accepted as one of the reasons why composites formed by initial MPs addition have lower protection values than the composites made by adding MPs later. According to Figure 13, when the PPy amount in PET/MPs/PPy composites declines, the Ab values also decrease. In addition, MPs inhibit the PPy chain, reducing

conductivity and shielding value, resulting in a lower EMSE.

Due to the predominant presence of MnFe_2O_4 , PPy exhibited the most significant disruption in the conduction pathway, resulting in the highest surface resistivity. The initial ferrite coating series exhibited a high Mn content, which had a detrimental impact on conductivity (Table 1). However, the composite still demonstrated relatively high conductivity due to the subsequent pyrrole deposition, achieved most effectively on this fabric. Nevertheless, within the first deposition of PPy followed by MnFe_2O_4 , the fabric's conductivity experienced a decline as a result of the extensive penetration of PPy into the substrate, leading to disruptions in the conductivity pathways (Table 2). The PPy's ground surface exhibits the accumulation of magnetic particles. The conductive polymer exhibits a preference for the surface coated with ferrite.

Consequently, the present study yielded the highest PPy content, facilitating the introduction of a more incredible amount of ferrite with manganese. It is thought that PPy will exhibit a higher degree of deposition, particularly in areas with a higher concentration of manganese. However, due to the substantial quantity of conductive polymer present, it effectively counteracts the insulating properties of MnFe_2O_4 . In the context of the second deposition series (PET/PPy/ MnFe_2O_4), it is observed that despite the relatively low PPy content, a dense coating results in insulation. This is because the surface is deposited densely, thereby causing an interruption in the conduction paths. Thus, this phenomenon is evident in the outcomes of the EMSE values.

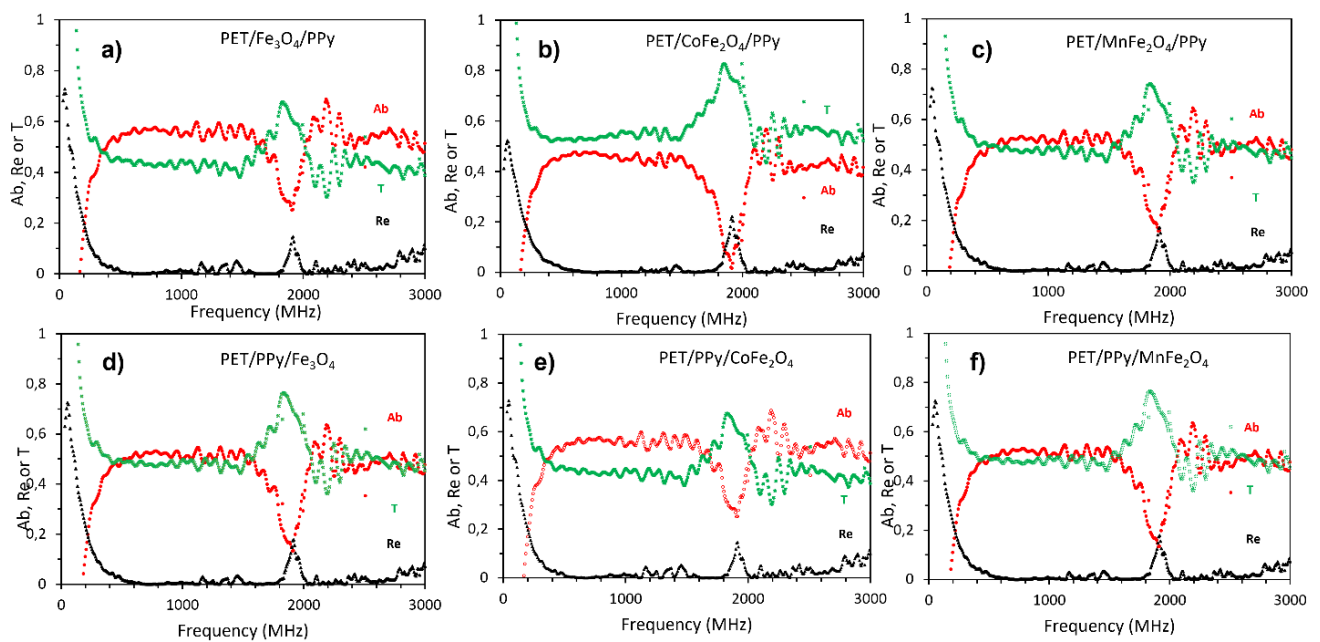


Figure 13. Ab, Re or T relative shielding efficiency of a)-c) PET/MPs/PPy composites, and d)-f) PET/PPy/MPs composites.

4. CONCLUSION

Through two distinct deposition procedures, it was proved that it is possible to modify the surface of PET nonwoven fabric with both conductive PPy and various MPs. According to the results, the composite manufacturing series using consecutive PPy and MPs deposition (PET/PPy/MPs) provided the best electrical conductivity values compared to the composites with reverse deposition. SEM micrographs demonstrated that altering the following deposition sequence resulted in the morphological

differentiation of the composites. Although the composite manufacturing series with sequential MPs and PPy deposition (PET/MPs/PPy) gave increased electrical conductivity, the EMSE values created in the opposite direction provided increased protection. One of the study's most significant findings was the EMI shielding performance of the PET/PPy/MPs composites, particularly the coated-PET/PPy/Fe₃O₄ composite, indicating the composite's future potential for the creation of technical textiles with EMI shielding properties.

REFERENCES

1. Pall ML. 2016. Microwave frequency electromagnetic fields (EMFs) produce widespread neuropsychiatric effects including depression. *Journal of Chemical Neuroanatomy* 75, 43-51.
2. Miller A B, Sears M E, Morgan L L, Davis D L, Hardell L, Oremus M, Soskolne C L. 2019. Risks to Health and Well-Being From Radio-Frequency Radiation Emitted by Cell Phones and Other Wireless Devices. *Frontiers in Public Health* 7, 223.
3. Avloni J, Ouyang M, Florio L, Henn A R, Sparavigna A J J o T C M. 2007. Shielding effectiveness evaluation of metallized and polypyrrole-coated fabrics. *Journal of Thermoplastic Composite Materials* 20(3), 241.
4. Yavuz Ö, Ram M, Aldissi M, Poddar P, Srikanth H. 2005. Polypyrrole composites for shielding applications. *Synthetic Metals* 151(3), 211-217.
5. Maity S, Singha K, Debnath P, Singha M. 2013. Textiles in electromagnetic Radiation Protection. *Journal of Safety Engineering* 2(2), 11-19.
6. Erdoğan M K, Karakişla M, Saçak M. 2012. Preparation, Characterization and Electromagnetic Shielding Effectiveness of Conductive Polythiophene/Poly(ethylene terephthalate) Composite Fibers. *Journal of Macromolecular Science Part A* 49(6), 473-482.
7. Kim M, Kim H, Byun S, Jeong S, Hong Y, Joo J, Song K, Kim J, Lee C, Lee J J S m. 2002. PET fabric/polypyrrole composite with high electrical conductivity for EMI shielding. *Synthetic Metals* 126(2-3), 233-239.
8. Yıldız Z, Usta I, Gungör A J T R J. 2012. Electrical properties and electromagnetic shielding effectiveness of polyester yarns with polypyrrole deposition. *Textile Research Journal* 82(20), 2137-2148.
9. Tunakova V, Gregr J, Tunák M, Dohnal G. 2016. Functional polyester fabric/polypyrrole polymer composites for electromagnetic shielding: Optimization of process parameters. *Journal of Industrial Textiles* 47(5), 686-711.
10. Rubeziene V, Abraitienė A, Baltušnikaitė-Guzaitienė J, Varnaite-Zuravliova S, Sankauskaitė A, Kancleris Z, Ragulis P, Šlekas G. 2018. The influence of distribution and deposit of conductive coating on shielding effectiveness of textiles. *The Journal of The Textile Institute* 109(3), 358-367.
11. Ammayappan L, Jose S, Chakraborty S, Pan N C. 2016. Conductive polymer based technical textiles from polyaniline. *Asian Dyer* 13(5), 65-70.
12. Jagatheesan K, Ramasamy A, Das A, Basu A. 2015. Fabrics and their composites for electromagnetic shielding applications. *Textile Progress* 47(2), 87-161.
13. Kuhn H H, Child A D, Kimbrell W C. 1995. Toward real applications of conductive polymers. *Synthetic Metals* 71(1-3), 2139-2142.
14. Hoghoghifard S, Mokhtari H, Dehghani S. 2018. Improving EMI shielding effectiveness and dielectric properties of polyaniline-coated polyester fabric by effective doping and redoping procedures. *Journal of Industrial Textiles* 47(5), 587-601.
15. Stempien Z, Rybicki T, Rybicki E, Kozanecki M, Szykowska M I. 2015. In-situ deposition of polyaniline and polypyrrole electroconductive layers on textile surfaces by the reactive ink-jet printing technique. *Synthetic Metals* 202, 49-62.
16. Abbasi A M R, Militky J. 2013. EMI Shielding Effectiveness of Polypyrrole Coated Glass Fabric. *Journal Of Chemistry and Chemical Engineering* 7(3), 256.
17. Unver I S, Durmus Z J I T o M. 2017. Magnetic and microwave absorption properties of magnetite (Fe₃O₄)@ conducting polymer (PANI, PPy, PT) composites. *IEEE Transactions on Magnetics* 53(10), 1-8.
18. Akman O, Kavas H, Baykal A, Durmus Z, Aktaş B, Sözeri H J J o s, magnetism n. 2013. Microwave Absorption Properties of BaFe₁₂O₁₉-TiO₂ Composite Coated with Conducting Polymer. *Journal of Superconductivity and Novel Magnetism* 26(4), 1369-1373.
19. Wencai Z, Hu X, Bai X, Zhou S, Yan J, Chen P. 2011. Synthesis and Electromagnetic, Microwave Absorbing Properties of Core-Shell Fe₃O₄-Poly(3, 4-ethylenedioxythiophene) Microspheres. *ACS Applied Materials & Interfaces* 3(10), 3839-3845.
20. Yan L, Wang X, Zhao S, Li Y, Gao Z, Zhang B, Cao M, Qin Y. 2017. Highly Efficient Microwave Absorption of Magnetic Nanospindle-Conductive Polymer Hybrids by Molecular Layer Deposition. *ACS Applied Materials & Interfaces* 9(12), 11116-11125.
21. Li B, Weng X, Wu G, Zhang Y, Lv X, Gu G. 2017. Synthesis of Fe₃O₄/polypyrrole/polyaniline nanocomposites by in-situ method and their electromagnetic absorbing properties. *Journal of Saudi Chemical Society* 21(4), 466-472.
22. Li L, Li M, Qi S. 2017. Preparation and microwave absorption properties of silver-coated Nd-deposited strontium ferrite hollow microspheres with polypyrrole composites. *Journal of Materials Science: Materials in Electronics* 28, 4288-4294.
23. Khairy M, Gouda M E. 2015. Electrical and optical properties of nickel ferrite/polyaniline nanocomposite. *Journal of Advanced Research* 6(4), 555-562.
24. Yang H, Ye T, Lin Y, Liu M. 2015. Excellent microwave absorption property of ternary composite: Polyaniline-BaFe₁₂O₁₉-CoFe₂O₄ powders. *Journal of Alloys and Compounds* 653, 135-139.
25. Zhao H, Hou L, Lu Y J M, Design. 2016. Electromagnetic interference shielding of layered linen fabric/polypyrrole/nickel (LF/PPy/Ni) composites. *Materials & Design* 95, 97-106.
26. Zhao H, Hou L, Lu Y. 2016. Electromagnetic shielding effectiveness and serviceability of the multilayer structured cuprammonium fabric/polypyrrole/copper (CF/PPy/Cu) composite. *Chemical Engineering Journal* 297, 170-179.
27. Firoz Babu K, Dhandapani P, Maruthamuthu S, Anbu Kulandainathan M. 2012. One pot synthesis of polypyrrole silver nanocomposite on cotton fabrics for multifunctional property. *Carbohydrate Polymers* 90 (4), 1557-1563.
28. Engin Sagirli F, Kayali E, Sarac A. 2018. Polypyrrole/barium titanate/poly(acrylonitrile-co-methylacrylate)-deposited cotton fabrics: Electromagnetic shielding. *Journal of Industrial Textiles* 47(5), 656-673.
29. Elnahrawy A, Haroun A, Hamadneh I, Al-Dujaili A, kamel S. 2017. Conducting Cellulose/TiO₂ composites by in Situ Polymerization of Pyrrole. *Carbohydrate Polymers* 168, 182-190.

30. Maráková N, Humpolíček P, Kašpárková V, Capáková Z, Martinková L, Bober P, Trchová M, Stejskal J. 2017. Antimicrobial activity and cytotoxicity of cotton fabric coated with conducting polymers, polyaniline or polypyrrole, and with deposited silver nanoparticles. *Applied Surface Science* 396, 169-176.
31. Yörük A E, Erdoğan M K, Karakışla M, Saçak M. 2021. Deposition of electrically-conductive polyaniline/ferrite nanoparticles onto the polypropylene nonwoven for the development of an electromagnetic interference shield material. *The Journal of The Textile Institute* 113(2), 2660-2672.
32. Khalil M I J A J o C. 2015. Co-precipitation in aqueous solution synthesis of magnetite nanoparticles using iron (III) salts as precursors. *Arabian Journal of Chemistry* 8(2), 279-284.
33. Babayan V, Kazantseva N E, Moučka R, Stejskal J. 2017. Electromagnetic shielding of polypyrrole-sawdust composites: polypyrrole globules and nanotubes. *Cellulose* 24(8), 3445-3451.
34. Kaynak A, Beltran R. 2003. Effect of synthesis parameters on the electrical conductivity of polypyrrole - coated poly (ethylene terephthalate) fabrics. *Polymer international* 52(6), 1021-1026.
35. Beck F, Braun P, Oberst M. 1987. Organic electrochemistry in the solid state - overoxidation of polypyrrole. *Berichte der Bunsengesellschaft für physikalische Chemie* 91(9), 967-974.
36. Najar S S, Kaynak A, Foitzik R C. 2007. Conductive wool yarns by continuous vapour phase polymerization of pyrrole. *Synthetic Metals* 157(1), 1-4.
37. Lei J, Cai Z, Martin C R. 1992. Effect of reagent concentrations used to synthesize polypyrrole on the chemical characteristics and optical and electronic properties of the resulting polymer. *Synthetic Metals* 46(1), 53-59.
38. Lu X, Mao H, Zhang W. 2009. Fabrication of core - shell Fe₃O₄/polypyrrole and hollow polypyrrole microspheres. *Polymer Composites* 30(6), 847-854.
39. Guo R, Jiang S, Yuen C, Ng M. 2009. Microstructure and electromagnetic interference shielding effectiveness of electroless Ni-P plated polyester fabric. *Journal of Materials Science: Materials in Electronics* 20(8), 735-740.
40. Malhotra U, Maity S, Chatterjee A J J o A P S. 2015. Polypyrrole - silk electro - conductive composite fabric by in situ chemical polymerization. *Journal of Applied Polymer Science* 132(4).
41. Li X, Cao M, Li S, Li L, Yang Y, Liu R, Sun Z, Mo L, Xin Z, Chen Y, Li Y, Fang Y, Qi Y. 2022. In-Situ Oxidative Polymerization of Pyrrole Compositing with Cellulose Nanocrystal by Reactive Ink-Jet Printing on Fiber Substrates. *Polymers* 14(19), 4231.
42. Nagappan S, Ha C-S. 2015. Emerging trends in superhydrophobic surface based magnetic materials: fabrications and their potential applications. *Journal of Materials Chemistry A* 3(7), 3224-3251.
43. Harifi T, Montazer M. 2015. A robust super-paramagnetic TiO₂: Fe₃O₄: Ag nanocomposite with enhanced photo and bio activities on polyester fabric via one step sonosynthesis. *Ultrasonics sonochemistry* 27, 543-551.
44. Somvanshi S B, Kharat P B, Khedkar M V, Jadhav K. 2020. Hydrophobic to hydrophilic surface transformation of nano-scale zinc ferrite via oleic acid coating: magnetic hyperthermia study towards biomedical applications. *Ceramics International* 46(6), 7642-7653.
45. Subbaiah Munagapati V, Wen H-Y, Gollakota A R K, Wen J-C, Shu C-M, Andrew Lin K-Y, Tian Z, Wen J-H, Mallikarjuna Reddy G, Zyryanov G V. 2022. Magnetic Fe₃O₄ nanoparticles loaded papaya (Carica papaya L.) seed powder as an effective and recyclable adsorbent material for the separation of anionic azo dye (Congo Red) from liquid phase: Evaluation of adsorption properties. *Journal of Molecular Liquids* 345, 118255.
46. Hedayati K, Azarakhsh S, Ghanbari D. 2016. Synthesis and magnetic investigation of cobalt ferrite nanoparticles prepared via a simple chemical precipitation method. *Journal of Nanostructures* 6(2), 127-131.
47. Vignesh R H, Sankar K V, Amaresh S, Lee Y S, Selvan R K. 2015. Synthesis and characterization of MnFe₂O₄ nanoparticles for impedometric ammonia gas sensor. *Sensors and Actuators B: Chemical* 220, 50-58.
48. Zhang H, Liu Y, Zhou Y. 2014. Preparation of magnetic PET fabric loaded with Fe₃O₄ nanoparticles by hydrothermal method. *The Journal of The Textile Institute* 106(10), 1078-1088.
49. Dey S, Kar A K. 2019. Morphological and optical properties of polypyrrole nanoparticles synthesized by variation of monomer to oxidant ratio. *Materials Today: Proceedings* 18, 1072-1076.
50. Varshney S, Singh K, Ohlan A, Jain V, Dutta V, Dhawan S. 2012. Synthesis, characterization and surface properties of Fe₂O₃ decorated ferromagnetic polypyrrole nanocomposites. *Journal of Alloys and Compounds* 538, 107-114.
51. Li L, Xiang C, Liang X, Hao B. 2010. Zn_{0.6}Cu_{0.4}Cr_{0.5}Fe_{1.46}Sm_{0.04}O₄ ferrite and its nanocomposites with polyaniline and polypyrrole: Preparation and electromagnetic properties. *Synthetic Metals* 160(1-2), 28-34.
52. Kulkarni G, Kandesar P, Velhal N, Kim H, Puri V. 2021. Facile synthesis of coral cauliflower-like polypyrrole hemispheres toward screening electromagnetic interference pollution. *Journal of Applied Polymer Science* 138(22), 50447.
53. Saini P. 2015. Intrinsically conducting polymer-based blends and composites for electromagnetic interference shielding: Theoretical and experimental aspects. John Wiley & Sons, Inc., Hoboken, NJ, USA, Edition.
54. Dhawan S, Ohlan A, Singh K. 2011. Designing of nano composites of conducting polymers for EMI shielding, *Advances in Nanocomposites-Synthesis, Characterization and Industrial Applications*, InTech.
55. Huo J, Wang L, Yu H. 2009. Polymeric nanocomposites for electromagnetic wave absorption. *Journal of Material Science* 44(15), 3917-3927.